IOPscience iopscience.iop.org

Home Search Collections Journals About Contact us My IOPscience

The metallic transport of $(TMTSF)_2X$ organic conductors close to the superconducting phase

This article has been downloaded from IOPscience. Please scroll down to see the full text article.

2011 J. Phys.: Condens. Matter 23 345702

(http://iopscience.iop.org/0953-8984/23/34/345702)

View the table of contents for this issue, or go to the journal homepage for more

Download details:
IP Address: 132.210.207.16
The article was downloaded on 22/08/2011 at 19:40

Please note that terms and conditions apply.

IOP PUBLISHING JOURNAL OF PHYSICS: CONDENSED MATTER

J. Phys.: Condens. Matter **23** (2011) 345702 (8pp) doi:10.1088/0953-8984/23/34/345702

The metallic transport of $(TMTSF)_2X$ organic conductors close to the superconducting phase

P Auban-Senzier[1], D Jérome[1], N Doiron-Leyraud[2], S René de Cotret[2], A Sedeki[2], C Bourbonnais[2], L Taillefer[2], P Alemany[3], E Canadell[4] and K Bechgaard[5]

[1] Laboratoire de Physique des Solides, UMR 8502 CNRS Université Paris-Sud, 91405 Orsay, France
[2] Département de Physique and RQMP, Université de Sherbrooke, Sherbrooke, QC, J1K 2R1, Canada
[3] Departament de Química Física and Institut de Química Teòrica i Computacional (IQTCUB), Universitat de Barcelona, Diagonal 647, 08028 Barcelona, Spain
[4] Institut de Ciència de Materials de Barcelona (CSIC), Campus de la UAB, 08193 Bellaterra, Spain
[5] Department of Chemistry, HC Ørsted Institute, Copenhagen, Denmark

E-mail: pascale.senzier@lps.u-psud.fr, denis.jerome@lps.u-psud.fr, ndl@physique.usherbrooke.ca, cbourbon@physique.usherbrooke.ca, ltaillef@physique.usherbrooke.ca, p.alemany@ub.edu and canadell@icmab.es

Received 9 May 2011, in final form 30 June 2011
Published 12 August 2011
Online at stacks.iop.org/JPhysCM/23/345702

Abstract

Comparing resistivity data of the quasi-one-dimensional superconductors $(TMTSF)_2PF_6$ and $(TMTSF)_2ClO_4$ along the least conducting $c^\star$-axis and along the high conductivity a-axis as a function of temperature and pressure, a low temperature regime is observed in which a unique scattering time governs the transport along both directions of these anisotropic conductors. However, the pressure dependence of the anisotropy implies a large pressure dependence of the interlayer coupling. This is in agreement with the results of first-principles density functional theory calculations implying methyl group hyperconjugation in the TMTSF molecule. In this low temperature regime, both materials exhibit for ρ_c a temperature dependence $aT + bT^2$. Taking into account the strong pressure dependence of the anisotropy, the T-linear ρ_c is found to correlate with the suppression of the superconducting T_c, in close analogy with ρ_a data. This work reveals the domain of existence of the three-dimensional coherent regime in the generic $(TMTSF)_2X$ phase diagram and provides further support for the correlation between T-linear resistivity and superconductivity in non-conventional superconductors.

(Some figures in this article are in colour only in the electronic version)

1. Introduction

As seen in figure 1, the close proximity between superconductivity (SC) and an antiferromagnetic phase (AF/SDW (spin density wave)) is a key feature of the temperature–pressure phase diagram of the $(TM)_2X$ series (where TM is an electron donating organic molecule such as TMTTF or TMTSF and X is a monoanion) of organic conductors [1–3]. This situation is observed for all members of the family with anions $X = PF_6$, AsF_6, ReO_4, ... when the nesting of the quasi-one-dimensional Fermi surfaces is destroyed under a pressure near the critical pressure P_c and a non-magnetic metallic state becomes the new ground state. Because superconductivity exists mostly on the metallic side of this magnetic instability it is important to understand the nature of this metallic ground state. Recently, one of its striking features was brought forward, namely the existence of a temperature dependence of the longitudinal resistivity, ρ_a behaving like $aT + bT^2$, at odds with the standard Fermi liquid description of metals [4–6]. Furthermore, the T-linear contribution to

 © 2011 IOP Publishing Ltd Printed in the UK & the USA

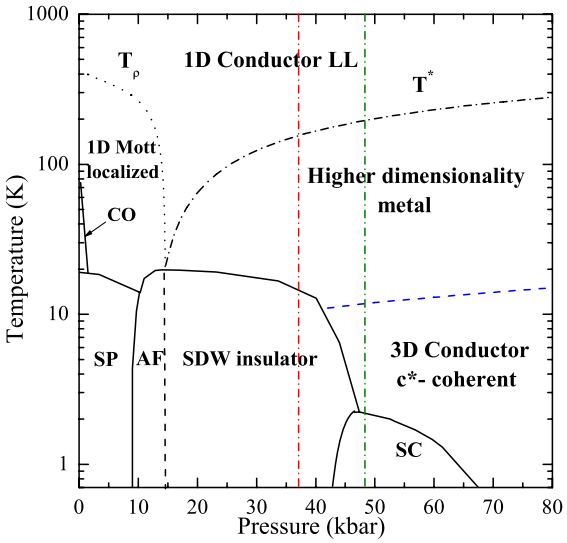

Figure 1. Generic temperature–pressure phase diagram of $(TM)_2X$. The origin of the pressure scale refers to the $(TMTTF)_2PF_6$ compound. The vertical dashed–dotted lines at 37 and 48 kbar are the estimated locations of $(TMTSF)_2PF_6$ and $(TMTSF)_2ClO_4$ under ambient pressure, respectively. In $(TMTSF)_2PF_6$, the SDW order vanishes at a pressure $P_c = 9.4$ kbar [3] whereas for $(TMTSF)_2ClO_4$ this critical point is located at negative pressures. The dashed line indicates the crossover between the high temperature quasi-1D and the low temperature coherent regimes, as discussed in the main text.

the resistivity was found to be directly correlated with the superconducting T_c in close analogy with cuprate [7] and iron-pnictide superconductors [8, 9]. This finding is surprising enough to warrant the performance of all possible additional confirmations on these superconducting materials using other samples.

The present study reports new measurements on different samples of the transverse transport along the least conducting $c^\star$-axis (i.e. normal to the *ab* plane), ρ_c, and addresses the comparison between ρ_a and ρ_c as a function of pressure and temperature. The $c^\star$-axis is, in the literature, the preferred direction for most transport studies since it provides easier and more reliable measurements of the resistivity [10–12].

Earlier works have revealed a $c^\star$-axis transport that goes from an insulating to a metallic temperature dependence at a temperature $T^\star$ taken as the signature of a crossover between two regimes [11, 13, 14]: a one-dimensional (1D) high temperature regime and, at low temperature, the regime of a higher dimensionality metal. The present work focuses on the low temperature domain where a 3D anisotropic coherent band picture prevails, in accordance with the observation of a transverse Drude edge [15] at liquid helium temperature. An important result of this investigation is the finding of an unexpectedly large pressure dependence for the interlayer coupling along $c^\star$, leading in turn to a significant drop of the ρ_c/ρ_a anisotropy under pressure.

2. ρ_c/ρ_a anisotropy and the 3D coherent regime

The $(TMTSF)_2PF_6$ and $(TMTSF)_2ClO_4$ single crystals used for the $c^\star$-axis measurements had two contacts evaporated on both *ab* planes and had room temperature resistivities of 50 and 28 Ω cm, respectively. These samples were measured with their *a*-axis counterparts in the same pressure cell, allowing a comparison of the temperature dependence of ρ_a and ρ_c at exactly the same pressure points for the two different samples. Experiments were performed at eight successive pressures from 8.4 up to 20.8 kbar for $(TMTSF)_2PF_6$ and six successive pressures from 1.5 up to 17 kbar for $(TMTSF)_2ClO_4$. A slow cooling rate ($\lesssim$5 K h^{-1}) was used below 50 K to ensure adequate thermalization and to optimize the anion ordering in $(TMTSF)_2ClO_4$. The experimental set up has been detailed in [4, 5].

The main purpose of this study is to look for the influence of the nearby magnetically ordered state on the electron scattering rate in the metallic phase. The SDW phase is actually the stable ground state in the phase diagram of $(TMTSF)_2PF_6$ up to the critical pressure $P_c = 9.4$ kbar [16, 3] and this critical point can be approached by adequate control of the pressure. For $(TMTSF)_2ClO_4$, the conducting state is stable at ambient pressure although a magnetic phase is never far away since it can be stabilized whenever the Fermi surface is left unfolded by the anion disorder [17, 18]. Consequently, the critical pressure of $(TMTSF)_2ClO_4$ cannot be determined and is assumed to be negative (see the vertical lines in figure 1).

In both materials, a polynomial analysis, already used for ρ_a data [5, 6] and to be detailed in section 3, enables us to determine at every pressure a residual resistivity ρ_{0c} in order to determine the temperature dependent inelastic scattering $\Delta\rho_c = \rho_c - \rho_{0c}$. The same quantity is also determined for ρ_a: $\Delta\rho_a = \rho_a - \rho_{0a}$.

Subsequently, in figure 2 we compare the inelastic contribution to the resistivity for current along the *a* and $c^\star$ axes, for $(TMTSF)_2PF_6$ at 11.8 kbar and $(TMTSF)_2ClO_4$ at 4.9 kbar. It is remarkable that both directions reveal similar temperature dependences up to 12 K and 30 K in $(TMTSF)_2PF_6$ and $(TMTSF)_2ClO_4$ respectively. This behaviour allows us to define a unique scattering time at low temperature governing both components of transport (a 3D coherent regime) and an anisotropy $\Delta\rho_c/\Delta\rho_a$ which is the ratio between the left and right scales in figure 2.

To the best of our knowledge, the upper limit for the 3D coherent regime and its pressure dependence have not yet been addressed in these quasi-1D conductors. We notice in figure 2 the interesting feature that the resistance along $c^\star$ looks 'more metallic' than the resistance along *a* when the temperature rises above the coherent regime. This is understood in terms of the particular crossover in these 1D conductors where at high temperature ρ_c is insulating, increasing on cooling, due to the 1D physics [11, 19]. A metallic behaviour for ρ_c is recovered only below the $T^\star$ crossover.

From our data, a fully coherent regime prevails at temperatures below 12 K in $(TMTSF)_2PF_6$ when both components of the resistivity exhibit similar temperature dependences. This upper limit for transverse coherence should be bounded by the kinetic coupling, t_c, along $c^\star$. This coupling is presumably very small compared to the coupling along the other directions.

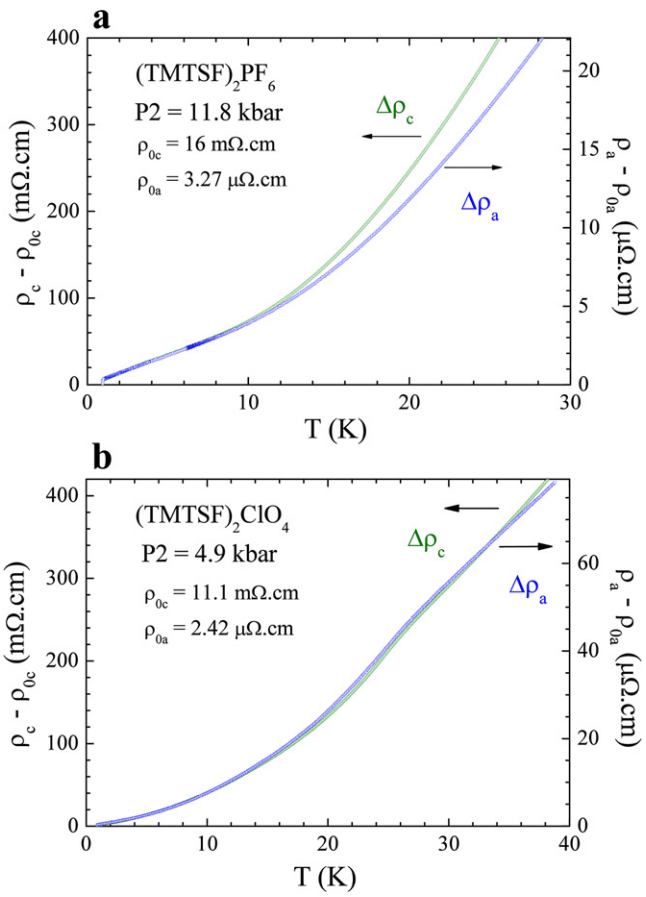

Figure 2. (a) Temperature dependence of $\rho_c - \rho_{0c}$ and $\rho_a - \rho_{0a}$ for $(TMTSF)_2PF_6$ under 11.8 kbar. Similar data have been obtained at every pressure up to 20.8 kbar. These data show the onset of an increase of the anisotropy around 12 K at 11.8 kbar, a temperature which increases up to 15 K for the two highest pressures. At the same time, $\Delta\rho_c/\Delta\rho_a$ at 10 K (the ratio between the left and right scales) decreases from 18 400 at 11.8 kbar down to 7400 at 19 kbar. (b) Temperature dependence of $\rho_c - \rho_{0c}$ and $\rho_a - \rho_{0a}$ for $(TMTSF)_2ClO_4$ under 4.9 kbar. These data show that, for $(TMTSF)_2ClO_4$, in contrast to $(TMTSF)_2PF_6$, $\Delta\rho_c/\Delta\rho_a$ at 10 K is only 5300 (the ratio between the left and right scales) and that the onset of an increase of the anisotropy starts above 30 K.

The temperature domain above t_c might actually correspond to the weakly-incoherent regime of 2D conductors [20, 21] in which Kohler's rule [22] as well as angular magnetoresistance oscillations are still observed [23–27].

Determining the onset of the temperature dependent anisotropy at different pressures enables us to draw an estimate for the upper limit of the temperature domain in which the $c^\star$-axis motion is fully coherent, as seen in figure 1.

In figure 3 we show the pressure dependence of the anisotropy derived from the ratio $\Delta\rho_c/\Delta\rho_a$ in the coherent regime at 10 K. We see that the pressure dependence of the anisotropy is quite prominent in both compounds. Although we present these anisotropy data in the same figure for both compounds, it is difficult to compare absolute values obtained for $(TMTSF)_2PF_6$ and $(TMTSF)_2ClO_4$ since $\Delta\rho_c/\Delta\rho_a$ at 10 K depends on the absolute resistivities under ambient conditions (1 bar and 300 K). Nevertheless, the pressure dependence is reliable.

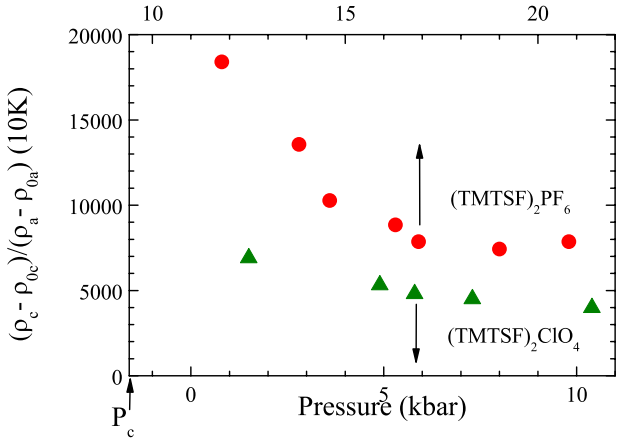

Figure 3. Pressure dependence of the anisotropy of resistivity $(\rho_c - \rho_{0c})/(\rho_a - \rho_{0a})$ measured in the coherent regime at 10 K. Data are displayed for $(TMTSF)_2PF_6$ (upper pressure scale) and $(TMTSF)_2ClO_4$ (lower pressure scale) with a shift of 11 kbar between the two pressure scales.

In the case of open Fermi surfaces [28] the anisotropy in the 3D coherent regime reads $\rho_c/\rho_a \propto (t_a/t_c)^2(a/c)^2$. Hence, such a large drop of the anisotropy is unexpected since a naive view could suggest the weak coupling between the *ab* planes to be less pressure dependent than the coupling along the chain axis.

Interestingly, the coupling along $c^\star$, although quite small, affects other physical properties which have been measured under pressure in both materials. The unnesting parameters of the band structure, t_b' and t_c', both play an important role in the *T*–*P* and *T*–*P*–*H* phase diagrams of $(TMTSF)_2X$.

First, when t_b' exceeds a critical unnesting band integral, the SDW ground state is suppressed in favour of a metallic phase with the possibility of restoration of SDW phases under magnetic field along $c^\star$ (FISDW for field-induced SDW) [28]. Second, the critical temperature for the stabilization of the FISDW subphases, $T_{\mathrm{FISDW}}(H)$, should be steadily increasing from zero in a 2D conductor or in a fully nested 3D conductor in the 'standard model' [29, 30]. However, since the real system is neither 2D nor perfectly nested ($t_c' \geq 0$), there exists a threshold field H_{T} for the appearance of FISDW subphases defined by $T_{\mathrm{FISDW}}(H_{\mathrm{T}}) = t_c'$ [31].

Early experiments on the FISDW of $(TMTSF)_2ClO_4$ under pressure at 1.5 K [32] revealed an increase of H_{T} of about 30% kbar^{-1}. Subsequent measurements on Bechgaard salts under pressure performed down to very low temperature did reveal a threshold field increasing from 4.5 T at 8 kbar to 8 T at 16 kbar on $(TMTSF)_2PF_6$ [26] and a somewhat similar pressure dependence in $(TMTSF)_2ClO_4$ [33]. Such a large pressure dependence of H_{T} implies a similarly large pressure dependence of t_c' within the 'standard model' with a concomitant increase of the interlayer coupling t_c.

As far as the absolute value of t_c is concerned, not much is known besides an early calculation published in 1983 for the case of $(TMTSF)_2ReO_4$, giving $t_c \approx 1$ meV [34]. In addition, an extended Hückel calculation has provided for $(TMTSF)_2PF_6$ a value of 0.8 meV for t_c [35]. Given the observed large pressure dependence of the $c^\star$ coupling it is

therefore important to see whether this pressure dependence can be explained by the pressure-induced deformation of the band structure.

3. Density functional theory calculation

First-principles calculations were carried out for $(TMTSF)_2PF_6$, for which reliable structural data have been obtained under 1 bar [36] and 6.5 kbar [37][6]. We used a numerical atomic orbital density functional theory (DFT) approach [38, 39] developed for efficient calculations in large systems and implemented in the SIESTA code [40]. The generalized gradient approximation to DFT and, in particular, the functional of Perdew, Burke and Ernzerhof was adopted [41]. Only the valence electrons are considered in the calculation, with the core being replaced by norm-conserving scalar relativistic pseudopotentials [42] factorized in the Kleinman–Bylander form [43]. We have used a split-valence double-ζ basis set including polarization orbitals as obtained with an energy shift of 10 meV for all atoms [44]. The energy cutoff of the real space integration mesh was 250 Ryd and the Brillouin zone was sampled using grids of $(4 \times 4 \times 4)$ k-points [45].

The calculated band structure under 6.5 kbar is reported in figure 4. The main parameters of the band structure at both 6.5 kbar and 1 bar are also given in that figure. Using the full band dispersion at the Γ point we obtain for t_a an increase of 0.88% kbar^{-1}. Although to the best of our knowledge there are no direct experimental data for comparison, this value matches well a previous more qualitative estimation by Ducasse *et al* [46], 0.75%. Concerning the effective transverse interaction t_b, let us note that taking the values of figure 4 for the $\Gamma \rightarrow Y$ line it looks as if t_b was decreasing from 1 bar to 6.5 kbar, something not easily matching the idea that the nesting of the Fermi surface deteriorates under pressure leading to the suppression of the SDW instability. However, when the full Brillouin zone is explored it is found that when moving from the $\Gamma \rightarrow Y$ line there is progressive change which quite soon results in an inversion of this behaviour. In particular, all along the Fermi surface the effective transverse interaction increases under pressure. Thus, the DFT band structure of $(TMTSF)_2PF_6$ seems to capture well the essential features of its pressure dependence. Let us note that the same type of calculation has already provided interlayer dispersion values consistent with experimental results for other molecular metals like α-(BEDT–TTF)$_2$KHg(SCN)$_4$ [47] and β-(BEDT–TTF)$_2$I$_3$ [48].

Turning to a comparison between the anisotropy data displayed in figure 3 and theory we note that the results in figure 3 give a drop of the anisotropy by a factor of $\approx$2.6 between 1 bar and 6.5 kbar. Using the full band dispersion at the Γ point and the dispersion along the Γ–Z direction we notice that the square of the ratio of dispersions along a and c drops by a factor of 2.3 under 6.5 kbar. This is admittedly close to the experimental drop of 2.6 in figure 3. Consequently, the DFT calculation of the band structure under pressure supports the unexpected strong dependence of the anisotropy.

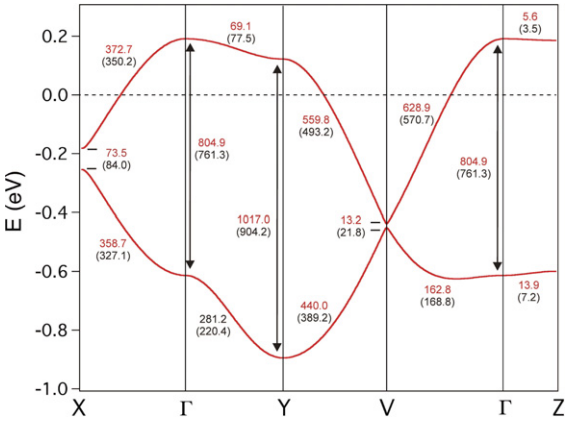

Figure 4. Calculated band structure for $(TMTSF)_2PF_6$ using the crystal structure obtained under 6.5 kbar. The bandwidths and gaps reported are for the structure under 6.5 kbar whereas the data in parentheses correspond to the 1 bar structure. All values are given in millielectronvolt. The dashed line refers to the Fermi level and $\Gamma = (0, 0, 0)$, $X = (1/2, 0, 0)$, $Y = (0, 1/2, 0)$, $V = (1/2, 1/2, 0)$ and $Z = (0, 0, 1/2)$ in units of the monoclinic reciprocal lattice vectors.

The origin of this result lies in the well known ability of methyl groups to propagate the π-type delocalization (hyperconjugation) through their π_{CH_3} and $\pi^*_{CH_3}$ orbitals [49]. Thus, even if weakly, the highest occupied molecular orbital (HOMO) of TMTSF extends towards the outer methyl groups. In the crystal structure of $(TMTSF)_2PF_6$ there are three short direct TMTSF interactions per dimer along the c direction which implicate these methyl groups. These contacts become shorter under pressure. For instance the C–C distances are 3.890, 3.890 and 3.971 Å at 1 bar and become 3.705, 3.705 and 3.936 Å at 6.5 kbar. In this way, the interlayer HOMO–HOMO interactions increase. Even if in absolute terms the effect is small, the inherent weakness of the interaction along c magnifies the variation and leads to the drop in the calculated values and in figure 3.

Assuming the unnesting coupling along c to be given by $t'_c = t_c^2/t_a$, the order of magnitude for its pressure dependence derived from the calculation amounts to 20% kbar^{-1}. This is admittedly in fair agreement with the observed strong pressure dependence of the FISDW onset field for both $(TMTSF)_2ClO_4$ and $(TMTSF)_2PF_6$, *vide supra*.

4. Correlation between ρ_c and T_c

We shall now develop the procedure used to analyse the temperature dependence of the transverse resistivity, ρ_c, from the raw experimental data.

The ρ_c data for $(TMTSF)_2PF_6$ at a pressure of 11.8 kbar, closest to P_c in our experiment, are displayed in figure 5(a) up

[6] A crystal structure under 9.8 kbar, which is however of somewhat lesser quality, was also reported in this reference and used in our study. However, when we compared the band structures at 1 bar, 6.5 and 9.8 kbar we detected a somewhat erratic behaviour for the HOMO bands of the last one in several parts of the Brillouin zone. Thus we concluded that the 9.8 kbar structure, although correctly describing most of the structural aspects, is not precise enough for the fine description of the band structure parameters.

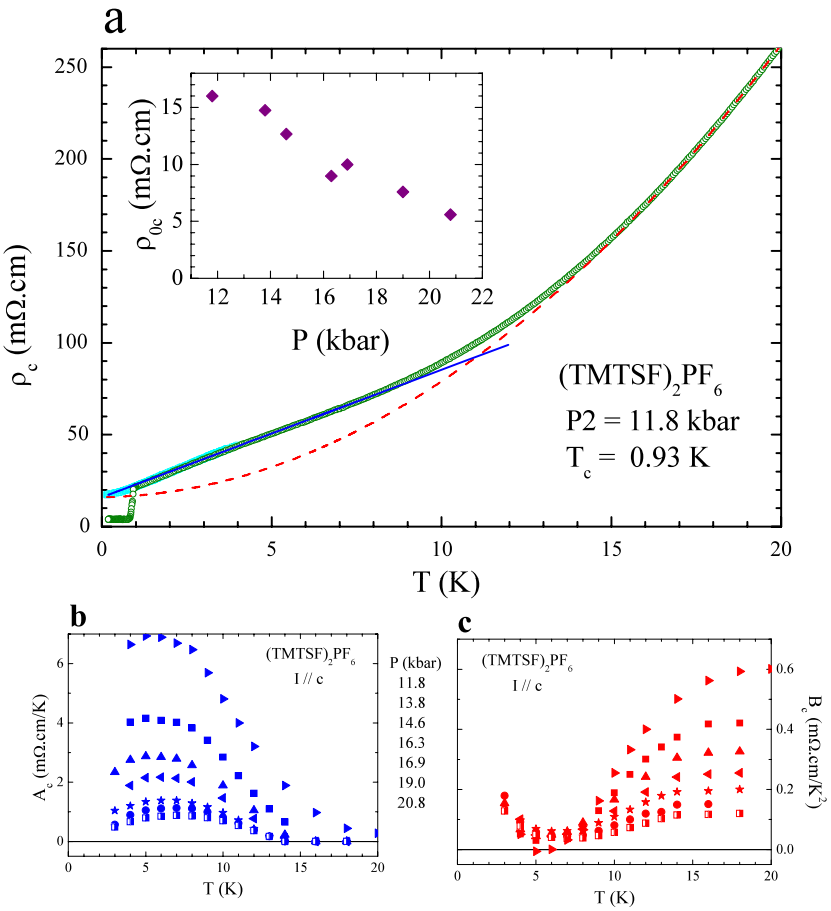

Figure 5. (a) $c^\star$-axis resistivity ρ_c of $(TMTSF)_2PF_6$ at 11.8 kbar versus temperature, at zero field and under $H = 0.05$ T applied along c^* in order to suppress superconductivity. The second order polynomial fit, $\rho_c(T) = \rho_{0,c} + A_c(T)T + B_c(T)T^2$, according to the sliding fit procedure described in the text, is shown for the T intervals 3–7 K (blue) and 18–22 K (dashed red). The inset displays the pressure dependence of the residual resistivity derived from the lowest temperature fit (see text). (b), (c) Temperature dependences of A_c and B_c at different pressures as indicated. Every temperature point corresponds to the centre of the 4 K window used for the fit.

to 20 K. We see that the resistivity can be analysed by the sum of an elastic contribution plus inelastic linear and quadratic contributions such that $\rho_c(T) = \rho_0 + A_cT + B_cT^2$. It is clear from the data shown in figure 5(a) that the relative weights of A_c and B_c are indeed changing with temperature, with A_c and B_c being dominant at low and high temperatures, respectively. A pure linear resistivity is observed at that pressure for the $c^\star$-axis transport below about 8 K, and down to about 0.3 K, by using a weak magnetic field of $H = 0.05$ T along $c^\star$ to suppress superconductivity. Above this linear regime, at about 15 K and above, the resistivity is quadratic in temperature, as indicated by the dashed red line in figure 5(a).

As far as $(TMTSF)_2ClO_4$ is concerned, see figure 6, the same polynomial analysis can be performed but it is more difficult to distinguish the purely linear or purely quadratic regimes. As shown in the resistivity data at 4.9 kbar displayed in figure 6(a), both inelastic contributions coexist over the entire temperature domain. In order to capture the evolution of A_c and B_c over the entire pressure and temperature range examined, we use the same sliding fit procedure employed in the context of in-chain data [5, 6], whereby we fit the resistivity curves to $\rho_c(T) = \rho_{0,c} + A_cT + B_cT^2$ over a sliding temperature window of 4 K. This fitting procedure has been carried out at all pressures keeping the value for the residual resistivity constant for all fits performed at a given pressure ($\rho_{0,c}$ is determined by the fit for the lowest temperature window). The result of this analysis on $(TMTSF)_2PF_6$ for all our measured pressures is shown in the bottom panels of figure 5 where the existence of a low temperature linear regime and a more quadratic high temperature regime is clear. Turning to the $(TMTSF)_2ClO_4$ data, this decomposition of the resistivity gives an excellent fit to the data over a large temperature range up to the anion ordering temperature with only a small variation of the fit parameters, as shown in the bottom panels of figure 6.

The sliding fit procedure gives nearly temperature independent prefactors for $(TMTSF)_2ClO_4$, but a strong temperature dependence is noticed in $(TMTSF)_2PF_6$, especially at the lowest pressures. The differences between the data for the two compounds may be ascribed to different distances from the critical point P_c. As a result, a stronger linear term can be anticipated in $(TMTSF)_2PF_6$, which is closer to P_c than $(TMTSF)_2ClO_4$, if the amplitude of the linear contribution is related to the proximity of the magnetic ground state. Moreover, $(TMTSF)_2ClO_4$ exhibits a folded Fermi surface which is likely to interfere with the development

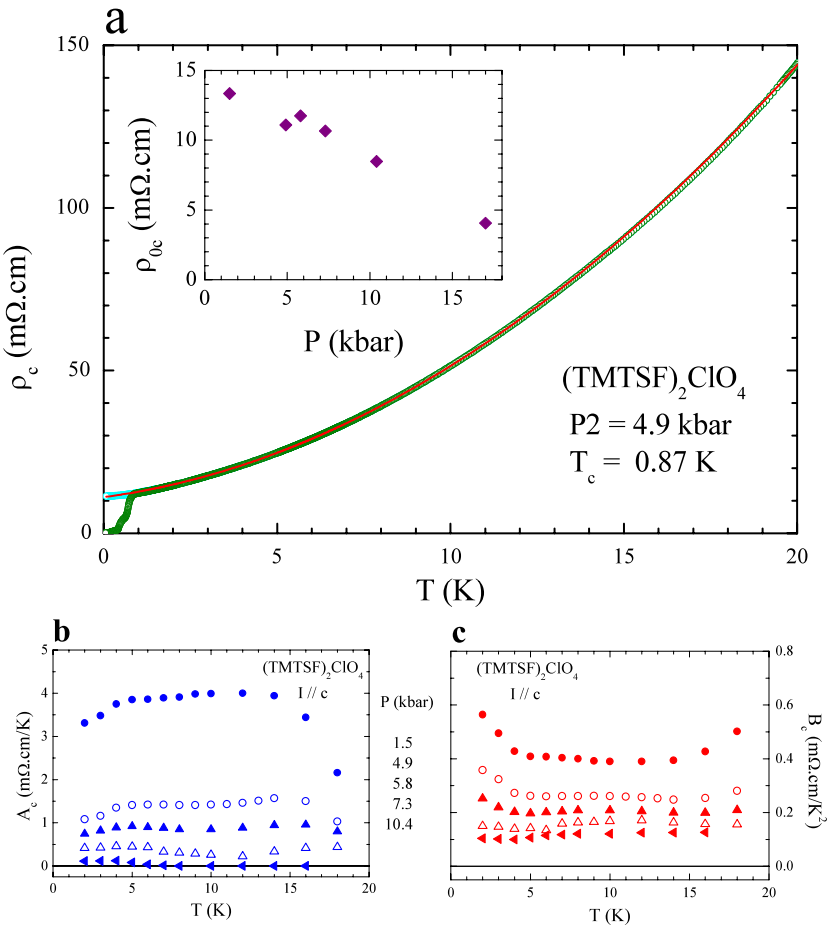

Figure 6. (a) $c^\star$-axis resistivity, ρ_c, of $(TMTSF)_2ClO_4$ at 4.9 kbar versus temperature, at zero field and under $H = 0.05$ T applied along $c^\star$ in order to suppress superconductivity. The second order polynomial fit, $\rho_c(T) = \rho_{0,c} + A_c(T)T + B_c(T)T^2$, described in the text is shown in red for the T interval 8–12 K. The inset displays the pressure dependence of the residual resistivity derived from the lowest temperature fit (see text). (b), (c) Temperature dependences of A_c and B_c at different pressures as indicated. Every temperature point corresponds to the centre of the 4 K window used for the fit.

of the linear contribution as obtained in $(TMTSF)_2PF_6$. At any rate, the present study of transport in the metallic phase of $(TMTSF)_2PF_6$ and $(TMTSF)_2ClO_4$ along the least conducting direction shows that the scattering rate comprises linear and quadratic terms, as seen for transport along the chains.

However, given the pressure dependence of the anisotropy displayed in figure 3 which is derived from the anisotropy of the inelastic scattering at low temperature one could expect the residual resistivity to show a similar effect. According to the insets of figures 5(a) and 6(a) the pressure dependence of the residual resistivity is significantly larger than that of the inelastic contribution. This feature can be understood as being because the residual resistance is quite sensitive to defects and was always found in the measurements of several samples to be less reliable than the measurements of temperature dependent resistance.

The decomposition of the inelastic scattering term as the sum of linear and quadratic terms rather than a power law suggests that a regular Fermi liquid scattering channel is superimposed on a more unusual one, the latter being most likely connected to the scattering on low energy spin fluctuations. It is worth noting that in the context of high-T_c cuprates, such superimposed scattering channels seem to give the best description of the normal-state resistivity data, such as reported for $Tl_2Ba_2CuO_{6+\delta}$ [50, 51] and $La_{2-x}Sr_xCuO_4$ [52]. It does not, however, necessarily require a 'two-fluid' like separation of the carriers (hot and cold regions on the Fermi surface for instance) as it can take place for one type of carriers when these are coupled to a wide fluctuation spectrum.

This has been indeed shown by scaling theory for the calculation of the electron–electron scattering rate close to SDW ordering in a quasi-1D metal (the results are summarized in [5]). Near the critical pressure, where the SDW connects with superconductivity, the spin fluctuations are strong and their spectrum is sharply peaked at a very low energy (ω_{sf}), which is comparable to or smaller than the temperature T (see, e.g., [54]). Under these conditions, their contribution yields a clear linear temperature dependence for the scattering rate, a known result for electrons interacting with low energy bosonic spin modes in two dimensions (see e.g., [55]). Moving away from the critical pressure, the spin fluctuations decrease, their spectral peak widens, drops in amplitude and gradually moves to much higher energy (an evolution confirmed on experimental grounds by the nuclear

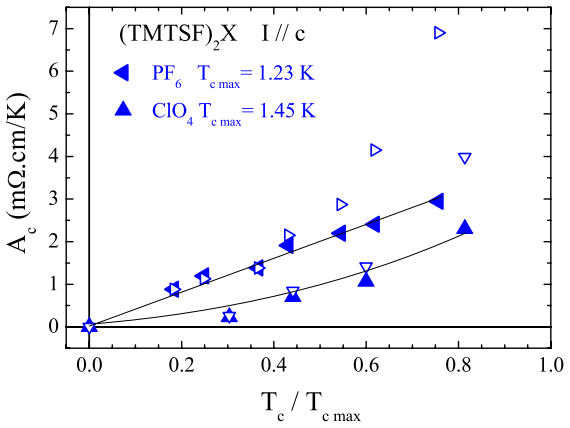

Figure 7. The A_c coefficient versus the reduced T_c in $(TMTSF)_2PF_6$ and $(TMTSF)_2ClO_4$; the empty symbols are the raw data for A_c determined at the temperature corresponding to its maximum value, namely, $T = 5$ K for $(TMTSF)_2PF_6$ and 10 K for $(TMTSF)_2ClO_4$; the full symbols are the A_c values corrected for the pressure dependence of the anisotropy (see text). The maximum T_c for $(TMTSF)_2PF_6$ is the value obtained at 8.4 kbar on the same sample, a pressure which is located in the inhomogeneous SDW/metal state. The maximum T_c for $(TMTSF)_2ClO_4$ comes from the ρ_c data at 1 bar obtained by Yonezawa [53] on a very slowly cooled sample from the same batch.

magnetic resonance spin-lattice relaxation rate under pressure in the Bechgaard salts [56, 57]). This corresponds to an intermediate situation where electrons scatter on both low and sizeable energy modes. The former modes are still responsible for a linear term, though with a decreasing amplitude under pressure, while the latter modes favour the opening of a different scattering channel at high energy which fulfils the Fermi liquid requirements ($\omega_{sf} \gg T$). Scaling theory calculations confirm that as one moves away from the critical pressure, the scattering rate is no longer perfectly linear in temperature above T_c, but develops some curvature that is fitted quite satisfactorily by an $aT + bT^2$ form (see figure 10 of [5]).

We have plotted in figure 7 the coefficient of the T-linear contribution, A_c, versus the reduced T_c ($T_c/T_{c\,max}$) for both compounds. Given that a significant contribution to the drop of A_c under pressure is actually due to the decrease of the anisotropy, it is of interest to plot the A_c coefficient corrected for the pressure-dependent anisotropy. In order to correct for this extrinsic drop of anisotropy under pressure we have divided the raw A_c values by the ratio of the anisotropy at each pressure point to the anisotropy at the highest pressure for each material (20.8 kbar for $(TMTSF)_2PF_6$ and 10.4 kbar for $(TMTSF)_2ClO_4$). We have neglected the pressure dependence of the band parameters given the very small variation of ρ_{0a} measured at the same time and shown in figure 4 of [5].

The result of this procedure, also plotted in figure 7, makes the dependence of A_c on T_c quasi-linear. This behaviour is in qualitative agreement with the renormalization group (RG) theory [5]. The present experiments do not approach the region very close to P_c (or the highest T_c) where a further enhancement of A_c, albeit nondiverging, is expected according to the one loop RG theory [5].

The vanishing of superconductivity of $(TMTSF)_2ClO_4$ above 8 kbar is likely due to the remanence of defects related to an incomplete anion ordering. Such a vanishing is not observed in $(TMTSF)_2PF_6$ which is expected to be a cleaner superconductor. Hence, superconductivity in $(TMTSF)_2PF_6$ persists up to the highest pressure of our study.

5. Conclusion

In summary, the investigation of the metallic region of the $(TMTSF)_2X$ phase diagram using the pressure and temperature dependence of the transverse resistivity ρ_c reveals several new features.

First, a comparison between ρ_a and ρ_c defines a domain of existence for a band-like motion of carriers along $c^\star$, namely below 12 K or so for $(TMTSF)_2PF_6$ and up to 30 K for $(TMTSF)_2ClO_4$, with a single scattering rate governing the temperature dependence of transport along a and $c^\star$, allowing a mapping of the 3D coherent regime.

Second, the anisotropy of resistivity in the 3D coherent regime reveals a strong pressure dependence which suggests a pressure dependence of the coupling much stronger along $c^\star$ than along a. Such a feature is actually in agreement with the pressure dependence of the FISDW phase diagram. This experimental behaviour is fairly well accounted for by the DFT band structure calculation performed according to the 1 bar and 6.5 kbar structures. The origin of the strong pressure dependence of the coupling along $c^\star$ lies in the well known ability of methyl groups to propagate π-type delocalization (hyperconjugation) through their π_{CH_3} and $\pi^*_{CH_3}$ orbitals.

Third, ρ_c has a temperature dependence departing from the canonical Fermi behaviour since a fit such as $\rho_0 + A_cT + B_cT^2$ provides a good description of the low temperature data, in contrast to the Fermi liquid T^2 law. When the pressure dependence of the anisotropy is taken into account the relation between A_c and T_c is similar to the relation found between A_a and T_c, in fair agreement with the RG one loop theory [5].

This work reinforces further the intimate connection between the two phenomena, also observed in cuprate and iron-pnictide high temperature superconductors [4, 58], suggesting that it is an essential ingredient for our understanding of these materials.

Acknowledgments

This work has been supported by NSERC (Canada), FQRNT (Québec), CFI (Canada), a Canada Research Chair (LT), the Canadian Institute for Advanced Research, CNRS (France) and DGI-Spain (Grants No. CSD2007-00041, FIS2009-12721-C04-03 and CTQ2008-06670-C02-02/BQU). We thank S Yonezawa for communicating ambient pressure data of a run on $(TMTSF)_2ClO_4$ performed at Kyoto.

References

[1] Jérome D and Schulz H J 1982 *Adv. Phys.* **31** 299
[2] Bourbonnais C and Jérome D 2008 *The Physics of Organic Superconductors and Conductors* ed A Lebed (Heidelberg: Springer) p 357

[3] Kang N, Salameh B, Auban-Senzier P, Jérome D, Pasquier C R and Brazovskii S 2010 *Phys. Rev.* B **81** 100509

[4] Doiron-Leyraud N, Auban-Senzier P, René de Cotret S, Bourbonnais C, Jérome D, Bechgaard K and Taillefer L 2009 *Phys. Rev.* B **80** 214531

[5] Doiron-Leyraud N, Auban-Senzier P, René de Cotret S, Bourbonnais C, Jérome D, Bechgaard K and Taillefer L 2010 *Eur. Phys. J.* B **78** 23

[6] Doiron-Leyraud N, Auban-Senzier P, René deCotret S, Bourbonnais C, Jérome D, Bechgaard K and Taillefer L 2010 *Physica* B **405** S265

[7] Daou R *et al* 2009 *Nature Phys.* **5** 31

[8] Fang L *et al* 2009 *Phys. Rev.* B **80** 140508

[9] Chu J H, Analytis J G, Kucharczyk C and Fisher I R 2009 *Phys. Rev.* B **79** 014506

[10] Korin-Hamzic B, Forro F and Cooper J R 1985 *Mol. Cryst. Liq. Cryst.* **119** 135

[11] Moser J, Gabay M, Auban-Senzier P, Jérome D, Bechgaard K and Fabre J M 1998 *Eur. Phys. J.* B **1** 39

[12] Naughton M J, Chamberlin R V, Chaikin P M, Yan X, Hsu S Y, Chiang L Y and Azbel M Y 1995 *Phys. Rev. Lett.* **61** 621

[13] Vescoli V, Degiorgi L, Henderson W, Grüner G, Starkey K P and Montgomery L K 1998 *Science* **281** 1181

[14] Giamarchi T 2004 *Quantum Physics in One-Dimension* (Oxford: Clarendon)

[15] Henderson W, Vescoli V, Tran P, Degiorgi L and Grüner G 1999 *Eur. Phys. J.* B **11** 365

[16] Vuletić T, Auban-Senzier P, Pasquier C, Tomič S, Jérome D, Héritier M and Bechgaard K 2002 *Eur. Phys. J.* B **25** 319

[17] Pouget J P, Shirane G, Bechgaard K and Fabre J M 1983 *Phys. Rev.* B **27** 5203

[18] Takahashi T, Bechgaard K and Jérome D 1982 *J. Physique Lett.* **43** L565

[19] Biermann S, Georges A, Lichtenstein A and Giamarchi T 2001 *Phys. Rev. Lett.* **87** 276405

[20] Kartsovnik M V, Andres D, Simonov S V, Biberacher W, Sheikin I, Kushch N D and Müller H 2006 *Phys. Rev. Lett.* **96** 166601

[21] Singleton J, Goddard P A, Ardavan A, Coldea A I, Blundell S J, McDonald R D, Tozer S and Schlueter J A 2007 *Phys. Rev. Lett.* **99** 027004

[22] Cooper J R, Forró L, Korin-Hamzić B, Bechgaard K and Moradpour A 1986 *Phys. Rev.* B **33** 6810

[23] Kang W, Hannahs S T and Chaikin P M 1992 *Phys. Rev. Lett.* **69** 2827

[24] Osada T, Kawasumi A, Kagoshima S, Miura N and Saito G 1991 *Phys. Rev. Lett.* **66** 1525

[25] Danner G M, Kang W and Chaikin P M 1994 *Phys. Rev. Lett.* **72** 3714

[26] Danner G M and Chaikin P M 1995 *Phys. Rev. Lett.* **75** 4690

[27] Sugawara S, Ueno T, Kawasugi Y, Tajima N, Nishio Y and Kajita K 2006 *J. Phys. Soc. Japan* **75** 053704

[28] Ishiguro T, Yamaji K and Saito G 1998 *Organic Superconductors* (Berlin: Springer)

[29] Héritier M, Montambaux G and Lederer P 1984 *J. Physique* **45** L943

[30] Héritier M 1987 *Low-Dimensional Conductors and Superconductors* ed D Jérome and L G Caron (New York: Plenum) p 243

[31] Montambaux G 1987 *Low-Dimensional Conductors and Superconductors* ed D Jérome and L G Caron (New York: Plenum) p 233
Montambaux G 1985 *PhD Thesis* Universitè d'Orsay

[32] Creuzet F, Jérome D and Moradpour A 1985 *Mol. Cryst. Liq. Cryst.* **119** 297

[33] Kang W, Hannahs S T and Chaikin P M 1993 *Phys. Rev. Lett.* **70** 3091

[34] Grant P M 1983 *J. Physique Coll.* **44** 847

[35] Balicas L, Behnia K, Kang W, Canadell E, Auban-Senzier P, Jérome D, Ribault M and Fabre J M 1994 *J. Physique* **4** 1539

[36] Thorup N, Rindorf G, Soling H and Bechgaard K 1981 *Acta Crystallogr.* B **37** 1236

[37] Gallois B, Gaultier J, Hauw C, Lamcharfi T-D and Filhol A 1986 *Acta Crystallogr.* B **42** 564

[38] Hohenberg P and Kohn W 1964 *Phys. Rev.* B **136** 864

[39] Kohn W and Sham L J 1965 *Phys. Rev.* A **140** 1133

[40] Soler J M, Artacho E, Gale J, García A, Junquera J, Ordejón P and Sánchez-Portal D 2002 *J. Phys.: Condens. Matter* **14** 2745

[41] Perdew J P, Burke K and Ernzerhof M 1996 *Phys. Rev. Lett.* **77** 3865

[42] Troullier N and Martins J L 1991 *Phys. Rev.* B **43** 1993

[43] Kleinman L and Bylander D M 1982 *Phys. Rev. Lett.* **48** 1425

[44] Artacho E, Sánchez-Portal D, Ordejón P, García A and Soler J M 1999 *Phys. Status Solidi* b **215** 809

[45] Monkhorst H J and Pack J D 1976 *Phys. Rev.* B **13** 5188

[46] Ducasse L, Abderrabba M, Hoarau J, Gallois B and Gaultier J 1986 *J. Phys. C: Solid State Phys.* **19** 3805

[47] Foury-Leylekian P, Pouget J P, Lee Y J, Nieminen R M, Ordejón P and Canadell E 2010 *Phys. Rev.* B **82** 134116

[48] Lee Y J, Nieminen R M, Ordejón P and Canadell E 2003 *Phys. Rev.* B **67** 180505

[49] Albright T A, Burdett J K and Whangbo M-H 1985 *Orbital Interactions in Chemistry* (New York: Wiley)

[50] MacKenzie A P, Julian S R, Sinclair D C and Lin C T 1996 *Phys. Rev.* B **53** 5848

[51] Proust C, Boaknin E, Hill R W, Taillefer L and Mackenzie A P 2002 *Phys. Rev. Lett.* **89** 147003

[52] Cooper R A *et al* 2009 *Science* **323** 603

[53] Yonezawa S, Maeno Y, Auban-Senzier P, Pasquier C, Bechgaard K and Jérome D 2008 *Phys. Rev. Lett.* **100** 117002

[54] Bourbonnais C and Sedeki A 2009 *Phys. Rev.* B **80** 085105

[55] Abanov A, Chubukov A V and Schmalian J 2003 *Adv. Phys.* **52** 119

[56] Creuzet F, Bourbonnais C, Caron L G, Jérome D and Moradpour A 1987 *Synth. Met.* **19** 277

[57] Brown S E, Chaikin P M and Naughton M J 2008 *The Physics of Organic Superconductors and Conductors* (*Springer Series in Materials Sciences*) ed A G Lebed (Berlin: Springer) pp 49–88

[58] Taillefer L 2010 *Annu. Rev. Condens. Matter Phys.* **1** 51